Method to Determine Tissue Fluorescence Efficiency *in Vivo* and Predict Signal-to-Noise Ratio for Spectrometers

E. V. TRUJILLO, D. R. SANDISON, U. UTZINGER, N. RAMANUJAM, M. FOLLEN MITCHELL, and R. RICHARDS-KORTUM *

Department of Electrical and Computer Engineering, The University of Texas, Austin, Texas, 78712. (E.V.T., U.U., N.R. and R.R-K.); Department 2665, Sandia National Laboratories, Albuquerque, New Mexico, 87185 (D.R.S.); and Department of Gynecologic Oncology, UT MD Anderson Cancer Center, Houston, Texas, 77035 (M.F.M.)

Recent clinical trials have demonstrated the potential of fluorescence spectroscopy for *in vivo* diagnosis of pathology. There is significant potential to reduce the cost and complexity of instrumentation to measure tissue spectra; however, careful analysis is required to maximize performance and minimize cost. One measure of performance is the signal-to-noise ratio (SNR) of the resulting data. This paper describes a method to predict the SNR of a given optical design for a particular tissue application. In order to calculate the expected SNR, two pieces of information are required: (1) the throughput and inherent noise of the system and (2) a quantitative relationship between the illumination energy and the resulting tissue fluorescence available for collection, which we define as the tissue fluorescence efficiency (FE). We present a method to calculate the fluorescence efficiency of tissue from *in vivo* measurements of tissue fluorescence. We report FE measurements of the normal and precancerous human cervix *in vivo* at 337, 380, and 460 nm excitation. We also present and evaluate a method to estimate the throughput and noise of various spectrometers and predict the expected SNR for tissue spectra by using the measured tissue FE. For squamous cervical tissue, as the degree of the disease increases, FE decreases, and as the excitation wavelength increases, FE decreases. Cervical tissue FE varies more than two orders of magnitude, depending on the tissue type and on the excitation wavelength used. Our SNR calculations, based on measured values of tissue FE, demonstrate agreement within a factor of 1.3 of the measured SNR on average. This method can be used to estimate the performance of different spectrometer designs for clinical use.

Index Headings: **Cost-effectiveness analysis; Cervix; Precancer; Fluorescence spectroscopy; Signal-to-noise ratio.**

INTRODUCTION

Recent clinical trials have demonstrated the potential of fluorescence spectroscopy for *in vivo* diagnosis of pathology.[1,2] Tissue fluorescence spectroscopy can be used to image large areas of tissue to identify areas suspicious for disease and extract diagnostically relevant structural and histochemical information.[3] This is an important advantage with respect to many traditional methods that require clinical expertise to identify areas to biopsy for subsequent histologic analysis. In particular, fluorescence has shown promise for the diagnosis of precancerous and cancerous lesions of the breast,[4] lung,[5] bronchus,[6] oral cavity,[7] cervix,[8] gastrointestinal tract,[1,9] and brain.[10]

Although spectroscopic measurements offer several advantages, instrumentation described in the literature is expensive relative to current diagnostic tools, and, in our experience, difficult for clinical staff to use without technical assistance. There is significant potential to reduce the cost and complexity of this instrumentation; however, careful analysis is required to maximize performance and minimize cost of instrumentation.

One measure of the performance of an optical system is the signal-to-noise ratio (SNR) of the resulting data. In general, as the SNR is reduced, the classification accuracy drops—as do the system costs.[11–13] This paper describes a method to predict the SNR of a given optical design for a particular tissue application and should serve as a guide in the design and evaluation of more cost-effective fluorescence diagnostic systems. We illustrate and validate this method with the particular example of detection of cervical precancer.

METHODS

In order to calculate the expected SNR for a given system design, two pieces of information are required: (1) the throughput and inherent noise of the system and (2) a quantitative relationship between the illumination energy and the resulting tissue fluorescence available for collection. In optically dilute samples, the quantum efficiency (QE) provides this relationship, and methods to measure QE are well known.[3] However, in turbid, multicomponent samples (such as tissue), these methods are not appropriate. To remove these limitations, we have developed a method to calculate the fluorescence efficiency (FE) of tissue from *in vivo* measurements of tissue fluorescence. We report fluorescence efficiency measurements of the normal and precancerous human cervix *in vivo* at three excitation wavelengths. We also present a method to estimate the throughput and noise of various spectrometers and predict the expected SNR for tissue spectra by using the measured fluorescence efficiency of tissue. We validate this method for cervical tissue fluorescence spectra.

FE Theory. In a dilute, homogeneous, nonscattering solution of pathlength L, Eq. 1 describes the relationship between the excitation energy ($P_0(\lambda_x)$) and the fluorescence energy arriving at the detector ($P(\lambda_x, \lambda_m)$), as a function of excitation and emission wavelength.

$$P(\lambda_x, \lambda_m) = \int_0^L dz\ P_0(\lambda_x)\mu_a(\lambda_x)\phi(\lambda_m)\beta(z). \qquad (1)$$

In this formula $\mu_a(\lambda_x)$ represents the absorption coefficient of the fluorophore at the excitation wavelength, $\phi(\lambda_m)$ is the fraction of absorbed energy converted to fluorescence at the emission wavelength, and $\beta(z)$ is the collection efficiency of the system, which depends on the

Received 3 November 1997; accepted 3 March 1998.
* Author to whom correspondence should be sent.

0003-7028/98/5207-0943$2.00/0

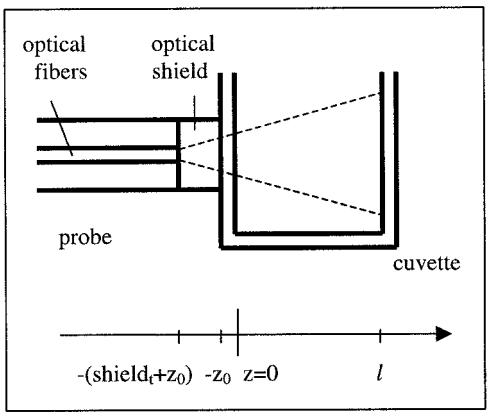

(a)

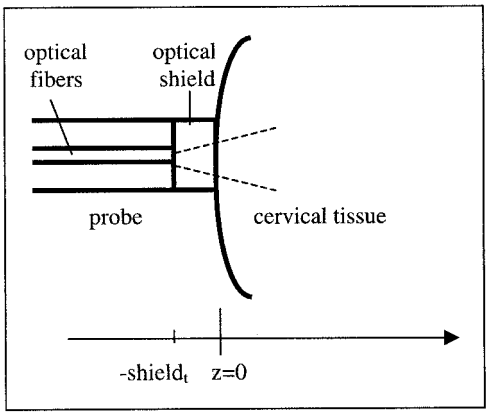

(b)

FIG. 1. Geometry of the fiber-optic probe used to measure fluorescence spectra of (**a**) standard solutions and (**b**) tissue.

depth along the optical axis, z. In the case where the collection efficiency is independent of z and has the value of β_0, Eq. 1 reduces to the familiar result:

$$P(\lambda_x, \lambda_m) = P_0(\lambda_x)\beta_0\mu_a(\lambda_x)\phi(\lambda_m)L. \quad (2)$$

Summing $\phi(\lambda_m)$ over all emission wavelengths yields the quantum efficiency of the fluorophore. The product of the absorption coefficient and the QE of an unknown fluorophore can be calculated from fluorescence measurements of the unknown sample and measurements from a sample with known absorption coefficient and QE; the measurements must be done with the same system under the same conditions. Derived from Eq. 1, the product of μ_a and the QE of the unknown is given by

$$\mu_{a\text{—unknown}}(\lambda_x)QE_{unknown} = \frac{\mu_{a\text{—known}}(\lambda_x)QE_{known}\sum_{\lambda_m} P_{unknown}(\lambda_x, \lambda_m)}{\sum_{\lambda_m} P_{known}(\lambda_x, \lambda_m)}. \quad (3)$$

If the absorption coefficient of the unknown is measured, the QE of the unknown can be computed.[3] The problem with this approach for tissue is that Eq. 1 is not valid for turbid media, since it does not include the effects of scattering and reabsorption present in turbid media. In a turbid sample, the fluorescence produced depends not only on the product of the absorption coefficient and the QE but also on the attenuation of excitation light propagating into the sample and the attenuation of fluorescent light propagating out of the sample. Furthermore, in most turbid media, the identity of fluorescent molecules is unknown. The absorption coefficient contains contributions from these fluorophores as well as other nonfluorescent chromophores. As a result, μ_a of the fluorophore cannot be determined easily in turbid media, in contrast to most dilute solutions where just one fluorophore influences this value. Finally, many tissues have a layered structure, and fluorophores and absorbers are not distributed homogeneously along the optical axis (z).

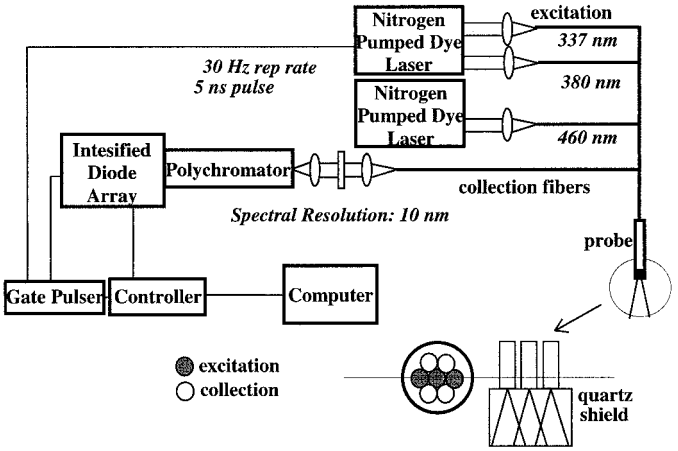

FIG. 2. Schematic diagram of the fluorimeter used to measure fluorescence spectra.

Although the QE is difficult to measure for turbid samples, it is relatively easy to measure the fluorescence efficiency, which describes the ratio of total emitted fluorescence energy to excitation energy. The fluorescence available to the detector from a turbid medium (P_t) containing a single fluorophore with absorption coefficient μ_a can be written as

$$P_t(\lambda_x, \lambda_m) = P_0(\lambda_x)\int_0^\infty dz\, H_{in}(\lambda_x, z)\mu_a(\lambda_x, z)\phi(\lambda_m, z) \times H_{out}(\lambda_m, z)\beta(z) \quad (4)$$

where $(H_{in}(\lambda_x, z))$ and $(H_{out}(\lambda_m, z))$ represent the sample attenuation of the excitation and emission light, respectively.

For a turbid medium containing multiple fluorophores, Eq. 4 can be generalized to

$$P_t(\lambda_x, \lambda_m) = P_0(\lambda_x)\int_0^\infty dz\, H_{in}(\lambda_x, z) \times \sum_k [\mu_{a_k}(\lambda_x, z)\phi_k(\lambda_m, z)]H_{out}(\lambda_m, z)\beta(z) \quad (5)$$

where the index k refers to individual fluorophores. We define the FE as

$$FE = \int_0^\infty dz \int_{\lambda_x}^\infty d\lambda_m H_{in}(\lambda_x, z) \sum_k [\mu_{a_k}(\lambda_x, z)\phi_k(\lambda_m, z)] \times H_{out}(\lambda_m, z). \quad (6)$$

As will be shown, the FE of an unknown turbid sample can be calculated from measurements of the unknown and measurements of a homogeneous sample with known optical properties (μ_a, QE) obtained by using a fiber-optic probe under similar conditions. Figure 1 shows a schematic diagram of the optical fiber probe used in these studies; multiple fibers were used to deliver excitation light and collect fluorescence through a transparent optical shield, with thickness $shield_t$. For turbid tissue measurements, the shield was placed directly in contact with the tissue. For standard measurements, the shield was placed in contact with the wall of a 1 cm thick quartz cuvette, with wall thickness z_0. Under these conditions, the fluorescence produced by an unknown turbid sample (P_t) and by a homogeneous standard (P_{std}) contained in a cuvette with wall thickness z_0 and pathlength ℓ, are given by Eqs. 7a and 7b, respectively,

$$P_t(\lambda_x, \lambda_m) = P_0 \int_0^\infty dz\ H_{in-t}(\lambda_x, z)\mu_{a-t}(\lambda_x)\phi_t(\lambda_m) \times H_{out-t}(\lambda_m, z)\beta_t(z) \quad (7a)$$

and

$$P_{std}(\lambda_x, \lambda_m) = P_0 \int_0^\ell dz\ H_{in-std}(\lambda_x, z)\mu_{a-std}(\lambda_x)\phi_{std}(\lambda_m) \times H_{out-std}(\lambda_m, z)\beta_{std}(z) \quad (7b)$$

where the subscript t refers to a turbid sample, in this case cervical tissue, and the subscript std refers to the reference standard used for the measurements. Assuming an isotropic fluorescence emission,[11] the collection efficiencies can be expressed as

$$\beta_t = \frac{\beta_0}{(z + shield_t)^2} \quad (8a)$$

and

$$\beta_{std} = \frac{\beta_0}{(z + shield_t + z_0)^2} \quad (8b)$$

where β_0 is a constant that includes the detector efficiency.

We further assumed that the tissue collection efficiency (β_t) was independent of z, since the depths from which most of the fluorescence is collected are very short (<300 μm)[15] compared to the shield thickness (1.7 mm) (Eq. 9).

$$\beta_t = \frac{\beta_0}{(shield_t)^2}. \quad (9)$$

Integrating both sides of the Eqs. 7a and 7b with respect to the emission wavelength, expressing their ratio, and using the collection efficiencies of Eqs. 8b and 9 provides a way to calculate the tissue FE, given the fluorescence spectrum of the tissue and a standard with known optical properties and collection geometry (see Eq. 10 below).

The FE of cervical tissue was estimated from *in vivo* measurements of tissue and subsequent measurements of a nonturbid standard, specifically, a Rhodamine 610 solution (2 mg/L in ethylene glycol), by using Eq. 10. The measurement techniques utilized for both the cervical tissue and the reference standard are described first, and then the FE calculation is presented.

Instrumentation. A schematic diagram of the portable fluorimeter, which was used to acquire the cervical tissue fluorescence and the reference standard spectra at three excitation wavelengths, is shown in Fig. 2. This system has been described in detail previously[16] and is briefly reviewed here. Two nitrogen-pumped dye lasers were used to provide illumination at three different excitation wavelengths: 337, 380, and 460 nm. Laser illumination at each excitation wavelength was coupled into the excitation fibers of the probe. Excitation light was delivered to the sample through a transparent optical shield with a thickness of 1.7 mm. The average transmitted pulse energies at the 337, 380, and 460 nm excitation wavelengths were 12, 9, and 14 μJ, respectively. The laser characteristics were a 5 ns pulse duration and a 30 Hz repetition rate. The proximal ends of the four emission collection fibers were arranged in a circular array and were imaged at the entrance slit of a polychromator, which was coupled to a 1024 intensified diode array that was controlled by a multichannel analyzer. Long-pass filters at 360, 400, and 470 nm were used to block the scattered light resulting from the 337, 380, and 460 nm excitation sources, respectively. During fluorescence measurements, a 205 ns collection gate, which was synchronized to the leading edge of the laser pulse with a pulser (Princeton Instruments PG 200), eliminated the effects of the white light used for visual examination.

Clinical Measurements. Clinical fluorescence spectra were measured from 374 cervical sites in a randomly selected group of 92 nonpregnant patients referred to the colposcopy clinic of the University of Texas MD Anderson Cancer Center on the basis of abnormal cervical cytology. Informed consent was obtained from each patient who participated, and the study was reviewed and approved by the Institutional Review Boards of the Uni-

$$FE_t(\lambda_x) = \left[\frac{\int_{\lambda_x}^\infty P_t(\lambda_x, \lambda_m)\, d\lambda_m}{\int_{\lambda_x}^\infty P_{std}(\lambda_x, \lambda_m)\, d\lambda_m}\right] \cdot \left[\frac{\int_0^\ell dz \int_{\lambda_x}^\infty d\lambda_m\ H_{in-std}(\lambda_x, z)\mu_{a-std}(\lambda_x)\phi_{std}(\lambda_m)H_{out-std}(\lambda_m, z)\frac{1}{(z + shield_t + z_0)^2}}{\frac{1}{(shield_t)^2}}\right]. \quad (10)$$

versity of Texas, Austin and the University of Texas, MD Anderson Cancer Center. Details of this clinical study have been described in detail previously but are briefly reviewed here.[16]

After colposcopic examination of the cervix, but before tissue biopsy, fluorescence spectra were acquired on average from two colposcopically abnormal sites, two colposcopically normal squamous sites, and one normal columnar site (if colposcopically visible) from each patient. Tissue biopsies were obtained only from abnormal sites identified by colposcopy and subsequently analyzed by the probe to comply with routine patient care procedures. All tissue biopsies were submitted for histologic examination by a panel of four board-certified pathologists, and a consensus diagnosis was established by using the Bethesda classification system.[17] Samples were classified as normal squamous (188 sites), normal columnar (26 sites), metaplasia (20), inflammation (25), low-grade squamous intra-epithelial lesion (LGSIL) (45 sites), or high-grade squamous intra-epithelial lesion (HGSIL) (70 sites).

Prior to each patient study, the probe was disinfected, and a background spectrum was acquired at all three excitation wavelengths consecutively with the probe dipped in a nonfluorescent bottle containing distilled water. The background spectrum was subtracted from all subsequently acquired spectra at corresponding excitation wavelengths for that patient. Next, measurements were taken with the probe placed on the face of a quartz cuvette containing a solution of a standard fluorophore molecule with known optical properties and QE. Rhodamine 610 dissolved in ethylene glycol (2 mg/L) was selected on the basis of its high quantum yield.[18] The concentration (2 mg/L) was adjusted empirically until the measured intensity of the Rhodamine standard was the same order of magnitude as typical tissue fluorescence. Other biological standards such as FAD and NADH were explored, but were found not to be stable over long periods of time. Fifty standard fluorescence spectra were measured at each excitation wavelength. After calibration, fluorescence spectra were acquired from the cervix: 10 spectra for 10 consecutive pulses were acquired at 337 nm excitation; and 50 spectra for 50 consecutive laser pulses were measured at 380 and 460 nm excitation. The probe was dipped in sterile water prior to measuring the fluorescence of the standard and each patient site to provide index matching between the tissue and the shield. All spectra were corrected for the nonuniform spectral response of the detection system by using correction factors obtained by recording the spectrum of an NIST (National Institute of Standards and Technology) traceable calibrated tungsten ribbon filament lamp.

FE Calculations. Equation 10 provides a method to calculate the FEs of all tissue samples. The first term in Eq. 10 can be calculated from the ratio of the total integrated fluorescence power of the tissue and the Rhodamine standard recorded before each patient's data. The second term in Eq. 10 requires knowledge of the optical properties of the standard as well as the collection geometry. Since the Rhodamine standard used was a nonscattering solution, and the numerical aperture of excitation and collection was small (NA = 0.22), the attenuation of excitation light entering and fluorescent light exiting the Rhodamine cuvette can be described with the Beer–Lambert law ($H_{in} = H_{out} = e^{-\mu_a(\lambda)z}$). The wavelength-dependent absorption coefficients of the Rhodamine standard were calculated from the measured Rhodamine absorbance. The quantum yield of Rhodamine 610 is 1.[18] The double integral in the second term of Eq. 10 can be evaluated numerically by using measured values of $\mu_a(\lambda_x)$, $\mu_a(\lambda_m)$, and $\phi(\lambda_m)$.

If $\phi(\lambda_m)$ is not known, but the quantum yield is known

$$\left(QE = \int_{\lambda_x}^{\infty} d\lambda_m \, \phi(\lambda_m)\right),$$

an alternative method can be used to calculate the FE. Eqs. 7a and 7b can be rewritten as

$$P_t(\lambda_x, \lambda_m) = P_0 \int_0^{\infty} dz \, H_{in\_t}(\lambda_x, z)\mu_{a\_t}(\lambda_x)\phi_t(\lambda_m) \times H_{out\_t}(\lambda_m, z)\frac{\beta_0}{(shield_t)^2} \quad (11a)$$

and

$$\frac{{}_{std}P_x(\lambda_m, \lambda_x)}{F(\lambda_m)} = P_0\mu_{a\_std}(\lambda_x)\phi_{std}(\lambda_m)\beta_0 \quad (11b)$$

where

$$F(\lambda_m) = \int_0^{\ell} dz \, H_{in\_std}(\lambda_x, z)H_{out\_std}(\lambda_m, z)(z + shield_t + z_0)^{-2}$$

and can be evaluated numerically at each emission wavelength. The FE can be then calculated by integrating both sides of Eq. 11, expressing their ratio, and replacing $\int d\lambda_m \, \phi_{std}(\lambda_m)$ by the known QE of the reference standard.

$$FE(\lambda_x) = \left[\frac{\int_{\lambda_x}^{\infty} d\lambda_m \, P_t(\lambda_x, \lambda_m)}{\beta_t}\right] \cdot \left[\frac{\mu_{a\_std}(\lambda_x)QE}{\int_{\lambda_x}^{\infty} d\lambda_m \frac{P_{std}(\lambda_x, \lambda_m)}{F(\lambda_m)}}\right]. \quad (12)$$

In this work, Eq. 12 was used to calculate the FE of all cervical tissue samples at each excitation wavelength. The method was tested by measuring the fluorescence efficiency of a nonscattering solution with known optical properties (0.1 g/L 1,1,4,4 tetraphenylbutadiene in cyclohexane) at 380 nm. Rhodamine was used as the reference standard. Two experiments were performed. In the first experiment the data from the tetraphenylbutadiene solution was taken by placing the probe on the wall of a 1 cm pathlength cuvette, similar to the Rhodamine standard acquisition (Fig. 1a). In the second experiment, the probe tip was placed in direct contact with the tetraphenylbutadiene solution in order to resemble the cervical tissue experiment setup. According to published values,[19] the quantum yield of a 0.1 g/L tetraphenylbutadiene in cyclohexane solution with an excitation wavelength of 365 nm is 0.6. The results were within 1% and 20% of this value for the first and second experimental protocols, respectively.

SNR Calculations. Using the FE of the 374 cervical

tissue sites, we calculated the expected signal-to-noise ratios for the spectrometer of Fig. 2 at each excitation wavelength (337, 380, and 460 nm). These were compared to measured SNRs of the 374 spectra at each excitation wavelength.

Predicted SNR. Calculation of the expected signal was carried out by estimating the losses in three stages: (1) excitation of fluorescence, (2) conversion to fluorescence, and (3) collection of fluorescence and conversion to electronic signal. The associated noise was then estimated, including readout noise, diode array dark charge noise, and photon shot noise. Finally, the SNR was estimated as the peak signal divided by the root mean square (rms) noise estimate. Although we report these calculations for the system of Fig. 2, the method is general in nature and can be applied to many different fluorimeters. A summary of all the abbreviations used in the SNR calculations, including definitions and typical values for the system in Fig. 2, is provided in Table I.

Estimating losses at the excitation stage permitted calculation of the incident energy on the tissue after all the transmission and coupling losses between the source and the excitation probe. The excitation energy, P_0 [J], was calculated as:

$$P_0 = P_{out} N_f T_q T_{fr} T_f \text{ [J]} \quad (13)$$

where P_{out} [J] represents the energy from the source, N_f is number of excitation fibers, T_q represents the internal transmission of the quartz coupling lenses at the excitation wavelength, T_{fr} is the fraction of energy remaining after all Fresnel losses at the air/glass interfaces, and T_f represents the internal fiber transmission.

To predict how much integrated tissue fluorescence power is available for collection (P_t), it is necessary to consider the energy incident on the tissue (P_0) and the cervical tissue FE:

$$P_t = P_0 \text{FE [J].} \quad (14)$$

To predict the amount of the available tissue fluorescence collected, the collection efficiency (CE) of the probe and the losses in the optics coupling the probe to the detector are estimated. Assuming isotropic fluorescence emission from a point source, the total integrated fluorescence collected at the probe (P_{probe}) is given by

$$P_{probe} = P_t T_q T_{fr} T_f \text{CE} \quad \text{[J]} \quad (15a)$$

and

$$\text{CE} = \beta_t = \frac{\pi R^2 n_f}{4\pi \text{shield}_t^2} \quad (15b)$$

where shield_t is the distance from the collection fiber to the tissue surface, R is the fiber radius, which is small compared to the shield thickness, and n_f is the number of collection fibers.

In order to calculate the fluorescence power incident on each element of the linear diode array detector (P_{diode}), all the collection system losses (optical losses, area mismatches, and dispersion of the fluorescence) are considered. The signal incident on each element of the diode can be estimated according to

$$P_{diode} = P_{probe} T_{fil} T_{gr} T_{NA} L_a L_{disp} \text{ [J/diode]} \quad (16)$$

TABLE I. Summary of parameter abbreviations used in SNR prediction and their typical values at 337 nm excitation wavelength. (The symbol * represents values that were calculated on the basis of a particular spectrum.)

Abbreviation	Meaning	Specifications for system in Fig. 2
BW	Bandwidth over which fluorescence is emitted	118 nm
$*C_{diode}$	Signal counts generated at each element of the linear diode array	1.4E4 counts
CE	Probe collection efficiency	0.0035
DC	Dark charge	70 counts/sec
Disp	Reciprocal linear dispersion	20 nm/mm
D	Pixel diameter	2.25E-3 cm
*FE	Cervical tissue fluorescence efficiency	0.003
$h\nu$	Energy per photon at the peak emission wavelength	4.5E-19 J
L_a	Signal fraction remaining after accounting for differences in the height of the dispersed spectrum and the height of the linear diode array	0.056
L_{disp}	Fraction of total integrated fluorescence incident on each diode	3.8E-3
$*N$	Total noise	120 counts
n_{accum}	Number of accumulations at each excitation wavelength	10 accumulations
N_{diode}	Diode array dark charge noise	5 counts
n_f	Number of collection fibers in the probe	4
N_f	Number of excitation fibers in the probe	1
$*N_{pb}$	Photon shot noise	120 counts
N_r	Readout noise	1 count
$*P_{diode}$	Energy incident on each element of the linear diode array	3.2E-14 J
$*P_{probe}$	Total integrated fluorescence collected by the probe	8.1E-10 J
$*P_o$	Energy incident on tissue	1.2E-4 J
$*P_{out}$	Energy from the source	1.7E-4 J
$*P_t$	Total fluorescence energy available for collection from the tissue	3.6E-7 J
$QE_{detector}$	Detector quantum efficiency	0.2
R	Fiber radius	0.01 cm
shield_t	Distance from tissue to the probe	0.17 cm
*SNR	Signal-to-noise ratio	120
t	Integration time per accumulation	10E-3 s
T_f	Internal fiber transmittance	0.93
T_{fil}	Filter transmittance	0.90
T_{fr}	Signal remaining after accounting for all Fresnel losses at the excitation and emission wavelengths	0.78, 0.72
T_{gr}	Grating efficiency	0.28
T_{NA}	Signal remaining after accounting for mismatch in probe and spectrograph NA	0.745
T_q	Internal lens transmittance at excitation and emission wavelengths	0.98, 0.96
T	Integration time	0.1 s
z_o	Cuvette wall thickness	0.127 cm

where T_{fil} represents the long-pass filter transmittance, T_{gr} represents the grating efficiency, T_{NA} describes the remaining signal after losses due to the mismatched numerical aperture of the probe and spectrograph, L_a describes the signal remaining after considering the mis-

TABLE II. Cervical tissue fluorescence efficiency minimum, maximum, and average values.

	337 nm Excitation			380 nm Excitation			460 nm Excitation		
	min	avg	max	min	avg	max	min	avg	max
Normal squamous	0.0001	0.0042	0.0156	6.1E-5	0.0011	0.0068	6.1E-5	0.0006	0.0038
Normal columnar	0.0004	0.0027	0.0056	2.9E-5	0.0007	0.0017	3.9E-5	0.0003	0.0009
Metaplasia	0.0005	0.0021	0.0053	0.0002	0.0005	0.0012	9.0E-5	0.0003	0.0010
Inflammation	0.0005	0.0022	0.0105	0.0001	0.0005	0.0018	7.4E-5	0.0004	0.0026
LG SIL	0.0002	0.0030	0.0120	3.1E-5	0.0008	0.0035	0.0001	0.0004	0.0026
HG SIL	0.0004	0.0026	0.0118	8.5E-5	0.0007	0.0033	3.3E-5	0.0003	0.0019

match in the height of the image at the back focal plane of the spectrograph and the height of the linear diode array, and L_{disp} describes the fraction of the total integrated fluorescence incident on each diode. L_{disp} was estimated as the ratio of the width of a diode, D, to the width of the dispersed spectrum, which is the product of the reciprocal linear dispersion, Disp, and the bandwidth over which fluorescence is emitted, BW, according to

$$L_{disp} = \frac{D}{\mathrm{Disp}^{-1}\mathrm{BW}}. \quad (17)$$

The light energy at each diode is then transduced to electronic counts (C_{diode}) according to

$$C_{diode} = \frac{P_{diode}}{h\nu}\mathrm{QE} \quad [\text{counts/diode}] \quad (18)$$

where $1/h\nu$ provides the conversion from energy to number of photons, and the $\mathrm{QE}_{detector}$ is the detector quantum efficiency in counts/photon.

Finally, the noise associated with this signal detection must be considered. In this case, three different types of noise are important: the shot noise associated with the signal (N_{ph}) for n_{accum} accumulations, the shot noise associated with the diode array dark charge (N_{diode}) for n_{accum} accumulations, and the detector read out noise (N_r) for n_{accum} accumulations.[20] The photon shot noise per pixel is modeled according to[20]

$$N_{ph} = \sqrt{C_{diode}} \quad [\text{counts/diode}]. \quad (19a)$$

When the diode array dark charge is measured, the associated noise contains contributions from both the shot noise associated with the dark charge and the readout noise associated with each accumulation. The shot noise of the dark charge is proportional to the square root of the dark charge per pixel, which was calculated from the detector specifications for dark charge per second (DC) in counts/s, and the total integration time (t [s]) per accumulation. The readout noise was estimated from the detector specifications and the number of accumulations (n_{accum}). Thus, the total noise associated with the diode array dark charge is described by Eq. 19b.

$$N_{diode} = \sqrt{n_{accum}\cdot(N_r^2 + \mathrm{DC}t)} \quad [\text{counts/diode}]. \quad (19b)$$

Since the diode array dark charge is subtracted from each measurement, the total noise estimate (N) is the root mean square of all noise types:

$$N = \sqrt{n_{accum}\cdot N_r^2 + N_{diode}^2 + N_{ph}^2} \quad [\text{counts}]. \quad (20)$$

Table I shows that, for the system in Fig. 2 (for cervical tissue), N is shot noise dominated. Finally, the expected SNR was calculated as

$$\mathrm{SNR} = \frac{C_{diode}}{N}. \quad (21)$$

In order to validate this method, the expected SNR was estimated for the system described previously by using measured FE values at each excitation wavelength for all the patient sites and compared to SNR results calculated from spectral measurements.

Measured SNR. In order to measure the SNR of a given spectrum, the noise present in the spectrum must be separated from the true signal. In this study, the collected data were oversampled in 0.5 nm increments, while the resolution of the clinical system was only 10 nm. One method to provide an estimate of the true signal is to sum adjacent pixels and resample the spectrum (binning). Consequently, in order to measure the SNR of the spectra, a moving average window of 20 data points (10 nm) was applied to each spectrum, providing P_{binned}, and subtracted from the original unbinned data, $P_{original}$, producing an estimate of the noise:

$$N = P_{original} - P_{binned}. \quad (22)$$

The noise was estimated at each emission wavelength

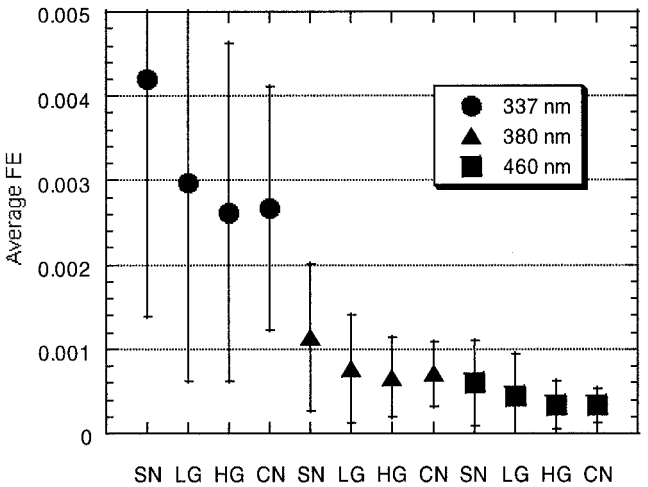

FIG. 3. Average FE (± standard deviation) for each tissue type at each excitation wavelength.

TABLE III. Ratio of maximum to minimum cervical tissue FEs.

Excitation wavelength (nm)	Average (max/min) per patient ±σ	(Max/min) all patients
337 nm	3.6 ± 3.3	135.8
380 nm	4.7 ± 7.9	232.4
460 nm	2.9 ± 2.4	115.9

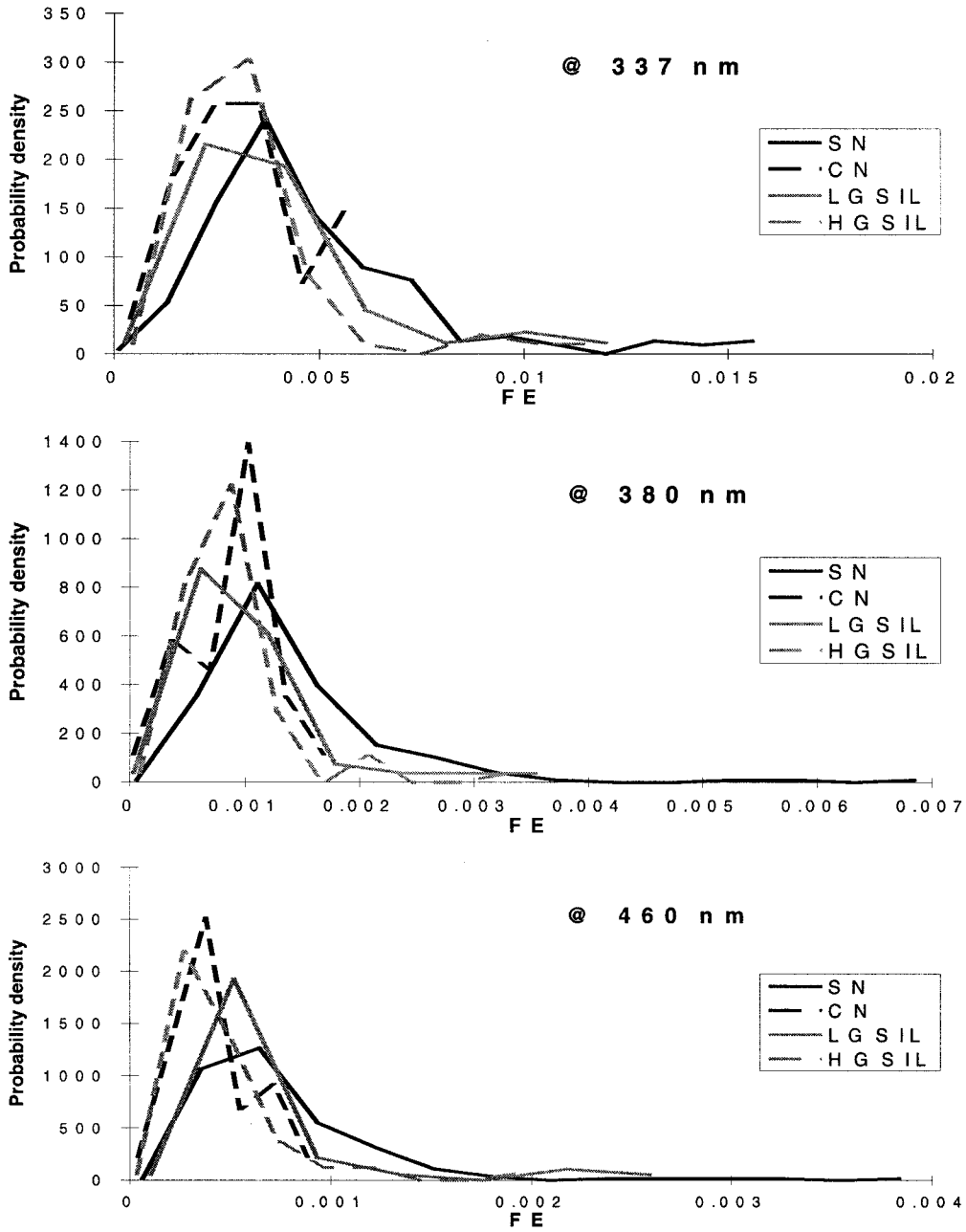

FIG. 4. Probability density functions for cervical tissue FE at 337, 380, and 460 nm excitation.

for the 374 patient sites spectra acquired at each excitation wavelength. To estimate the ratio of the signal to the root mean noise estimate (SNR), the binned signal was divided by the local standard deviation of the noise, computed from Eq. 22 at each point on the spectrum (Eq. 23). The standard deviation was locally obtained in the same moving window as the one used to calculate the moving average.

$$\mathrm{SNR} = \frac{P_{\mathrm{binned}}}{\sigma_{\mathrm{binned}}} \tag{23}$$

TABLE IV. Average predicted and measured SNRs, signals, and noise levels of spectra from 374 sites.

Excitation wavelength (nm)	Average SNR predicted $\pm\sigma$	Average SNR measured $\pm\sigma$	Average (signal predicted/ signal measured)	Average (noise predicted/ noise measured)
337	102 ± 43	105 ± 47	0.55 ± 0.30	0.55 ± 0.24
380	98 ± 48	105 ± 64	0.43 ± 0.24	0.46 ± 0.27
460	112 ± 61	85 ± 53	0.84 ± 0.56	0.62 ± 0.34

RESULTS AND DISCUSSION

FE Calculations. The FE was calculated at each excitation wavelength for each cervical site measured in all patients. The results of the FE calculations are shown in Table II and Fig. 3. The minimum, average, and maximum values of the FE calculated at the three different excitation wavelengths for each type of tissue are included in Table II. In Fig. 3, average values of the FE are

plotted for normal squamous (NS), normal columnar (NC), LGSIL, and HGSIL at each excitation wavelength. Standard deviations are shown as error bars. For squamous cervical tissues, the FE of the tissue decreases as the degree of the disease progresses. From high to low FE, the diagnostic categories are NS, LGSIL, HGSIL, and NC. As the excitation wavelength increases, the FE decreases.

The ratio of the maximum to the minimum cervical tissue FE at each excitation wavelength for all patients is indicated in two ways. Table III gives (1) the ratio for the entire data set of 374 spectra from 92 patients (max/min), and (2) the ratio of the maximum to the minimum FE for all sites from a given patient averaged over all patients (average(max/min)). The variability of the FE among all patients for a specific excitation wavelength is more than two orders of magnitude and is greatest at 380 nm. The ratio of the maximum to the minimum FE for all sites from a given patient, averaged over all patients, is much less (Table III). Within a patient, the cervical tissue FE varies less than an order of magnitude, and variation is greatest at 380 nm excitation again. This result indicates that, while the tissue FE varies significantly from patient to patient, it varies much less within a patient.

Relative frequency histograms of the FE for each type of tissue at each excitation wavelength are displayed in Fig. 4. In all cases, there is significant overlap between the FE distributions of various tissue types, indicating that the measurement of the FE by itself cannot be used as an accurate diagnostic value. At 337 and 380 nm excitation, the SN distribution is shifted toward higher FE values relative to the other tissue types. At 380 nm excitation, the LGSIL distribution is shifted toward lower FE values relative to the other tissue types. At 460 nm excitation, the HGSIL distribution is shifted toward lower FE values relative to the other tissue types.

SNR Calculations. Table I combined with Eqs. 13–21 represents the calculation of a typical SNR prediction. The listed values represent the system performance and fluorescence characteristics of a particular patient at 337 nm excitation. The symbol * designates that the value is derived from a particular patient spectrum. The results of Table I indicate a predicted SNR of 120. The measured SNR for the same patient was 124.

Table IV lists the average measured and predicted SNRs for the spectra from the 374 sites. The ratio of the average predicted to the average measured SNR is 0.97 at 337 nm, 0.93 at 380 nm, and 1.3 at 460 nm excitation. In addition, Table IV lists the ratio of the predicted signal to the measured signal and the ratio of the predicted noise to the measured noise averaged for all 374 sites. The average ratios of the predicted signal to the measured signal and the predicted noise to the measured noise range from 0.52 to 0.78 and from 0.45 to 0.60, respectively, indicating that the measured signal and noise are approximately twice the predicted signal and noise.

Anisotropic cervical tissue emission may contribute to the discrepancies between measured and predicted signal intensities, which employed an isotropic tissue emission assumption. Previous studies performed in arterial tissue have demonstrated empirically that tissue does not emit isotropically, as a result of highly forward scattering.[14,21] For arterial specimens, tissue fluorescence power decreases with the detector-to-sample separation distance, R, as $1/R^n$, where $n = 1.1$. The FE of cervical tissue in this investigation was calculated under the assumption that $n = 2$. For $n = 1.1$, the predicted signal is 2.7 times larger than the predicted signal for $n = 2$.

CONCLUSION

We have developed a method to calculate the fluorescence efficiency of tissue from *in vivo* measurements of tissue fluorescence. Cervical tissue FE varies more than two orders of magnitude, depending on the tissue type (NS, NC, LG, or HG) and on the excitation wavelength used (337, 380, and 460 nm in this investigation). As the excitation wavelength increases, the FE decreases. The FE decreases with increasing degree of disease for squamous cervical tissue.

General methods to estimate the SNR of acquired fluorescence data and to predict the expected SNR for tissue fluorescence spectra have been described in detail. This method was applied to cervical tissue fluorescence data obtained with a fiber-optic fluorescence spectrometer. The SNR predictions, based on measured values of tissue FE, demonstrate agreement within a factor of 0.97 at 337 nm, 0.93 at 380 nm, and 1.3 at 460 nm excitation to the measured SNRs, on average. This method can be used to predict the SNR expected for various spectrometer designs.

ACKNOWLEDGMENT

We gratefully acknowledge funding provided by the Whitaker Foundation.

1. R. M. Cothren, R. R. Richards-Kortum, M. V. Sivak, M. Fitzmaurice, R. P. Rava, G. A. Boyce, G. B. Hayes, M. Doxtader, R. Blackman, T. B. Ivanc, M. S. Feld, and R. E. Petras, Gastrointestinal Endoscopy **36,** 105 (1990).
2. N. Ramanujam, M. F. Mitchell, A. Mahadevan, S. Thomsen, and R. Richards-Kortum, Proc. Nat. Acad. Sci. U.S.A. **91,** 10193 (1994).
3. R. Richards-Kortum, ''Fluorescence Spectroscopy of Turbid Media'', in *Optical-Thermal Response of Laser-Irradiated Tissue,* A. J. Welch and M. J. van Gemert, Eds. (Plenum Press, New York, 1995), Chap. 20, p. 667.
4. R. R. Alfano, A. Pradhan, and C. G. Tang, J. Opt. Soc. Am. B **6,** 1015 (1989).
5. R. R. Alfano, G. C. Tang, A. Pradhan, W. Lam, D. S. C. Choy, and A. Opher, Quantum Electron. **23,** No. 10, 1806 (1987).
6. J. Hung, S. Lam, J. C. LeRiche, and B. Palcic, Lasers Surg. Med. **11,** 99 (1991).
7. K. Roy, I. Bottrill, D. R. Ingrams, M. M. Pankratov, E. Rebeiz, P. Woo, S. Shapshay, S. Kabani, R. Manoharan, I. Itzkan, and M. S. Feld, Proc. SPIE **2395,** 1135 (1995).
8. N. Ramanujam, M. F. Mitchell, A. Mahadevan, S. Thomsen, E. Silva, and R. Richards-Kortum, Gynecol. Oncol. **52,** 31 (1994).
9. K. T. Schomacker, J. K. Frisoli, C. C. Compton, T. J. Flotte, J. M. Richter, N. S. Nishioka, and T. F. Deutsch, Laser Surg. Med. **12,** 63 (1992).
10. S. Montan and L. G. Stromblad, Lasers Life Sci. **1,** 275 (1987).
11. B. K. Rutt and D. H. Lee, J. Magn. Res. Imag. **6,** 57 (1996).
12. D. A. Ortendahl and L. E. Crooks, Med. Prog. Technol. **15,** 171 (1989).
13. P. M. Parizel, H. A. Dijkstra, G. P. Geenen, P. A. Kint, R. J. Versteylen, P. J. van Wiechen and A. M. De Schepper, Eur. J. Radiol. **19,** 132 (1995).
14. K. Pope, S. Warren, Y. Yazdi, A. Johnston, M. Davis, and R. R. Richards-Kortum, ''Dual Imaging of Arterial Walls: Intravascular Ultrasound and Fluorescence Spectroscopy'', in *Proceedings of*

Biomedical Optics '93: Diagnostic and Therapeutic Cardiovascular Intervention III, (SPIE, Bellingham, Washington, 1993), pp. 1878–1906.
15. A. J. Welch, C. Gardner, R. Richards-Kortum, G. Criswell, E. Chan, J. Pfefer, and S. Warren, Lasers Surg. Med. (1997), paper in press.
16. N. Ramanujam, M. F. Mitchell, A. Mahadevan-Jansen, S. L. Thomsen, G. Staerkel, A. Malpica, T. Wright, N. Atkinson, and R. Richards-Kortum, Photochem. Photobiol. **64,** 4 (1996).
17. T. C. Wright, R. J. Kurman, and A. Ferenczy, ''Cervical Intraepithelial Neoplasia'', in *Pathology of the Female Genital Tract,* A. Blaustein, Ed. (Springer Verlag, New York, 1994), pp. 229–277.
18. D. G. Taylor and J. N. Demas, Anal. Chem. **51,** 712 (1979).
19. I. Berlman, *Handbook of Fluorescence Spectra of Aromatic Molecules* (Academic Press, New York, 1971).
20. Y. Talmi, ''Intensified Array Detectors'', in *Charge-Transfer Devices in Spectroscopy,* J. V. Sweedler, K. L. Ratzlaff, and M. B. Denton, Eds. (VCH Publishers, New York, 1994), Chap. 5, pp. 167–171.
21. S. Warren, K. Pope, Y. Yazdi, A. Johnston, M. Davis, and R. Richards-Kortum, ''Monte Carlo Fluorescence Verification of Experimental Results for the Combined Ultrasonic and Spectroscopic Imaging of Coronary Artery Disease,'' in *Proceedings of the 30th Annual Rocky Mountain Bioengineering Symposium* (IEEE, Piscataway, New York, 1993), pp. 457–458.